On the Use of the Climate Forecast System Reanalysis Wind Forcing In Ocean Response Modeling

Andrew T. Cox and Vincent J. Cardone
Oceanweather Inc., Cos Cob, Connecticut

Val R. Swail
Environment Canada, Toronto, Ontario, Canada

1. Introduction

The National Centers for Environmental Prediction (NCEP) have completed a new coupled global reanalysis known as the Climate Forecast System Reanalysis (CFSR). Like the original NCEP Reanalysis (R1/R2) performed in the 1990s (Kalnay, et al. 1996), the reanalysis provides surface marine wind fields suitable for ocean response modeling such as the application of a third-generation (3G) wave model. This paper describes specific assessment of the CFSR forcing and wave response in a number of meteorological regimes including extreme extra-tropical "winter hurricanes", tropical systems, and monsoonal flows. This paper is not intended as an all-inclusive validation and evaluation of the CFSR winds, but rather to inform potential users as to the applicability of the data and its use in ocean response modeling. Previous studies (Swail and Cox, 2000) have shown that advanced 3G wave models can produce nearly perfect simulations of the significant wave height when driven by accurate surface wind fields. Thus, a proven 3G wave model is also used to assess the skill in the wind fields.

2. CFSR Data

The NCEP CFSR (Saha, *et al.* 2010) is a new coupled global reanalysis which spans the period of 1979 to March 2011. The CFSR improves upon the original R1/R2 NCEP reanalysis in numerous ways including horizontal resolution (from ~200 km to ~38 km) and in coupling the atmospheric model with ocean and sea ice models. Data assimilation methods have been improved since the R1/R2 and, importantly for marine use, data from the ERS 1 and 2 (1991-1997), QUIKSCAT (2001-2009) and WINDSAT (Sept 2008-present) scatterometers has been assimilated into the CFSR analysis. Altimeter wind speed datasets, however, have not been assimilated (personal communication with CFS Team) and thus provide one of the best independent measures of winds over the global oceans. Full details on the CFSR can be found in Saha, *et al.* 2010, or on the CFSR website at http://cfs.ncep.noaa.gov/cfsr/.

Data are made available via the National Climatic Data Center NOMADS site (http://nomads.ncdc.noaa.gov/data.php?name=access#cfsr) or via the CISL Research data archive (http://dss.ucar.edu/pub/cfsr.html). Data on the NOMADS site were downloaded from the Gaussian T382 (approximately 38 km) hourly archive for the wnd10m (10 meter winds), tmp2m (2 meter surface temperature) and tmpsfc (surface/skin temperature) from the "Timeseries" datasets. Data are provided in monthly segment GRIB2 (GRIdded Binary) format files with one variable per file for the 1979-2009 time periods in the timeseries dataset. Data for January 2010 to March 2011 must be obtained from the "Hourly, Pressure, Fluxes, and Ocean Data" datasets on the NOMADS site which do not make available single variable files and thus require more time to download. The CFSR modeling system is not expected to be made available past March 2011 as version 2 of the modeling system was put in implementation.

While GRIB2 is a standard format for exchange of data between national weather centers, researchers may find it more convenient to convert CFSR data to netCDF using a utility such as WGRIB2 (http://www.cpc.ncep.noaa.gov/products/wesley/wgrib2/). The data archive is quite large; the 1979-2009 time period requires 266 GB for the wnd10m dataset and 174 GB each for the temperature fields. Temperature fields were required to derive the effective neutral wind from the CFSR archive using the algorithm described by Cardone *et al. (1990)* in order to provide proper wind forcing to the wave model.

3. Wave Model

The wave model used for this study is a discrete spectral type called OWI 3G (Oceanweather 3rd Generation). The spectrum is resolved at each grid point in 24 directional bins and 23 frequency bins. The bin centre frequencies range from 0.039 Hz to 0.32 Hz increasing in geometric progression with a constant ratio 1.10064. Deep-water physics is assumed in both the propagation algorithm and the source terms. The propagation scheme (Greenwood *et al*., 1985) is a downstream interpolatory scheme that is rigorously energy conserving with great circle propagation effects included. The source term formulation and integration is a third-generation type (WAMDI, 1988) but with different numerics and with the following modifications of the source terms in official WAMDI. First, a linear excitation source term is added to the input source term to allow the sea to grow from a flat calm condition without an artificial warm start sea state. The exponential wind input source is taken as the Snyder *et al*. (1981) linear function of friction velocity, as in WAMDI. However, unlike WAM, in which friction velocity is computed from the input 10-m wind speed following the drag law of Wu (1982), a different drag law is used in OWI 3-G. That law follows Wu closely up to wind speed of 20 m/s and then becomes asymptotic to a constant at hurricane wind speeds. The dissipation source term is taken

from WAMDI except that the frequency dependence is cubic rather than quadratic. Finally, the discrete interaction approximation to the non-linear source term is used as in WAMDI except that two modes of interaction are included (in WAMDI the second mode is ignored). Further details on this model and its validation may be found in Khandekar *et al*. (1994), Cardone *et al*. (1996) and Forristall and Greenwood (1998). This wave model has been shown to reproduce observed wave heights very well when driven by accurate wind fields (Cardone *et al*., 1995, 1996).

4. Validation Data

Altimeter wind speed and significant wave height data were obtained from the GlobWave archive (www.globwave.org) which provides a single archive of quality controlled-multiple platform altimeter data. The data has built in corrections to adjust individual platforms based on comparisons to co-located National Data Buoy Center buoy wind and wave measurements. The data set from 1991 to 2009 was applied which contains data from the TOPEX, ERS1, ERS2, ENVISAT, JASON-1, JASON-2 and GEOSAT follow-on satellite missions.

5. Case Studies

a. Global Wave Assessment

A global implementation of the OWI-3G wave model previously applied for the GROW (Global Reanalysis of Ocean Waves, see Cox and Swail, 2001) hindcast and as well as operational forecasts (see Cox and Cardone, 2002) was used to initially assess the overall global performance of the CFSR forcing. The model applied a 0.625 by 1.25 degree latitude-longitude grid and was driven with hourly CFSR wind fields (adjusted to neutral stability). A daily ice edge was applied in the model from CFSR ice concentration data. The model was run for the entire 1979-2009 time period, but assessment was restricted to the time period of available altimeter measurements (1991-2009).

The overall statistics shown in Table 1 indicate that the CFSR winds and CFSR/OWI-3G waves are overall very skillful. The assessment contains over 600 million matched pairs of hindcast and altimeter data points. There is a small negative bias (0.38 m/s) in the wind speeds overall with an excellent scatter index (standard deviation/mean measurement) of 20%. Wave results are even more impressive with just 8 cm positive bias and a scatter index of 18%. The overall wave results are, on average, in the same range of those obtained in the MSC50 hindcast (Swail,

et al. 2006) in the North Atlantic which applied wind fields from R1 and intensive kinematic analysis to result in a wave hindcast with just 4 cm bias and scatter index of 17%.

Quantile-quantile comparisons of the wind and waves shown in Figure 1 indicate that the CFSR winds and CFSR/OWI-3G waves represent the distribution of winds and waves measured by the altimeter well past the 99th percentile. It is suspected that altimeter wind saturation may play a part in the apparent over-estimation of the winds at the 99.8th and 99.9[th] percentiles when wind speeds exceed 20 m/s. Wave height comparisons are linear up to the 99.9[th] percentile, although these represent wave heights just under 10 meters where most modern 3rd generation model are expected to perform well. Wind speed and wave height bias binned by measurement (Figure 2) indicates that above 10 meters the CFSR winds and resulting waves are tending towards negative bias in higher sea-states.. This negative bias is a concern for applications that develop extreme design criteria which require accurate specification of peak conditions. Further discussion of the CFSR in strong forcing conditions associated with tropical and extra-tropical storms in included in sections 5C and 5D.

Table 1 Global CFSR wind and CFSR/OWI-3G wave statistics

```
                  Number    Mean    Mean    Diff     RMS   Stnd   Scat            Corr
                  of Pts    Meas    Hind    (H-M)   Error    Dev  Index  Ratio    Coeff
                 --------  ------  ------  ------   -----  -----  -----  -----    -----
Wind Spd. (m/s)  603113921   8.47    8.09   -0.38    1.71   1.66   0.20   0.22     0.94
Sig Wave Ht (m)  623817651   2.70    2.78    0.08    0.50   0.50   0.18   0.22     0.95
```
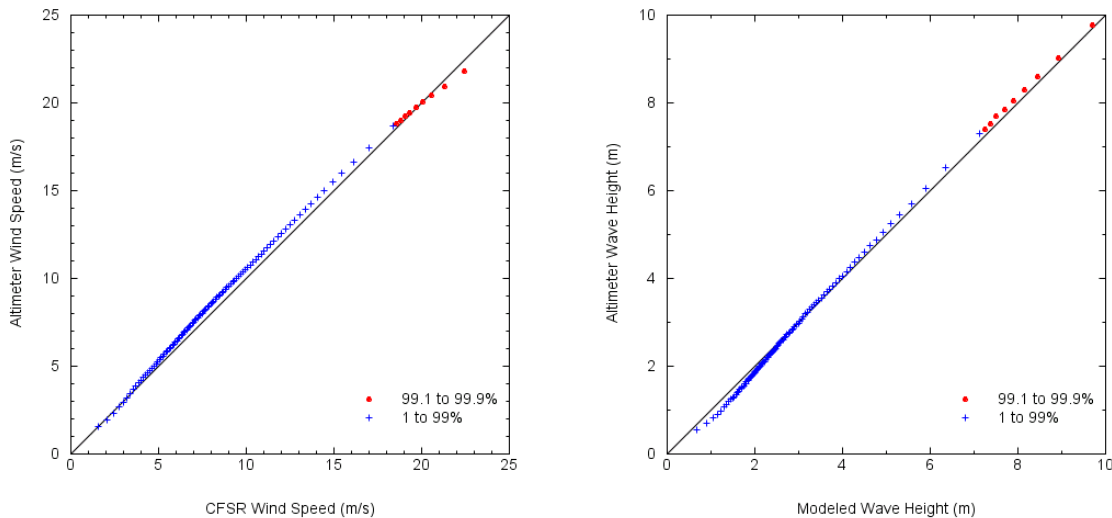

Figure 1 Global quantile-quantile (1 to 99.9%) comparison of CFSR/OWI-3G winds and waves against global altimeter measurements
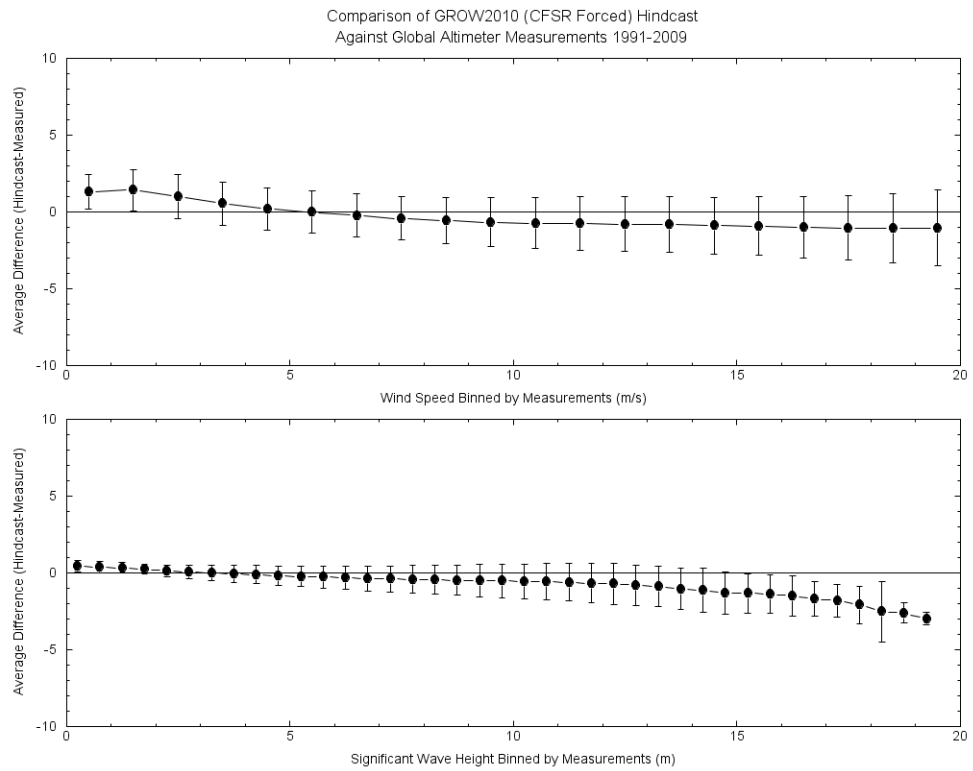
Figure 2 Comparison of wind (above) and wave (below) bias binned by altimeter measurement

b. Basin Assessment in WISPAC

The U.S. Army Corp of Engineers Wave Information Study Pacific hindcast (WISPAC) applied NRA wind fields which included regional and coastal statistical regressions based on measured data along with inclusion of tropical winds from a mesoscale model on a Pacific-wide 0.5 degree grid for the period 1980-2005. To assess the potential of CFSR for future WISPAC work, the CFSR wind data was compared to the same altimeter wind speed datasets used to evaluate WISPAC winds.

Wind statistics shown in Table 2 from the period 1991-2005 show that the CFSR provides an overall improvement in scatter index (24% vs. 29%) and correlation coefficient was improved from 82% to 87%. Figure 3 shows the mean wind speeds from the WISPAC, altimeter and CFSR from the co-located datasets along with plots of the mean bias (model-altimeter). This figure shows that most of the improvement in the CFSR wind data is in the Southern Hemisphere where the original NCEP reanalysis (on which the WISPAC was based) is known to have issues. Performance in the Northern Hemisphere is virtually identical.

To further evaluate the potential of CFSR for WISPAC, the OWI-3G model was setup on the WISPAC 0.5-degree grid covering the entire North and South Pacific oceans. Ice concentration data was supplied from the CFSR reanalysis and wave spectra from a global run were specified at the model boundaries.   Two continuous years with pickup conditions from a spin-up month were run for the year 2000 and 2004 representing a cold (2000) and warm (2004) Oceanic Nino Index (ONI) year based on Climate Prediction Center annual summaries. Wave statistics (Table 3) for the two-year run show similar improvement in scatter index and correlation coefficient for the resulting waves, with a larger contribution in the Southern Oceans.

Table 2 Altimeter Wind Statistics: 1991-2005

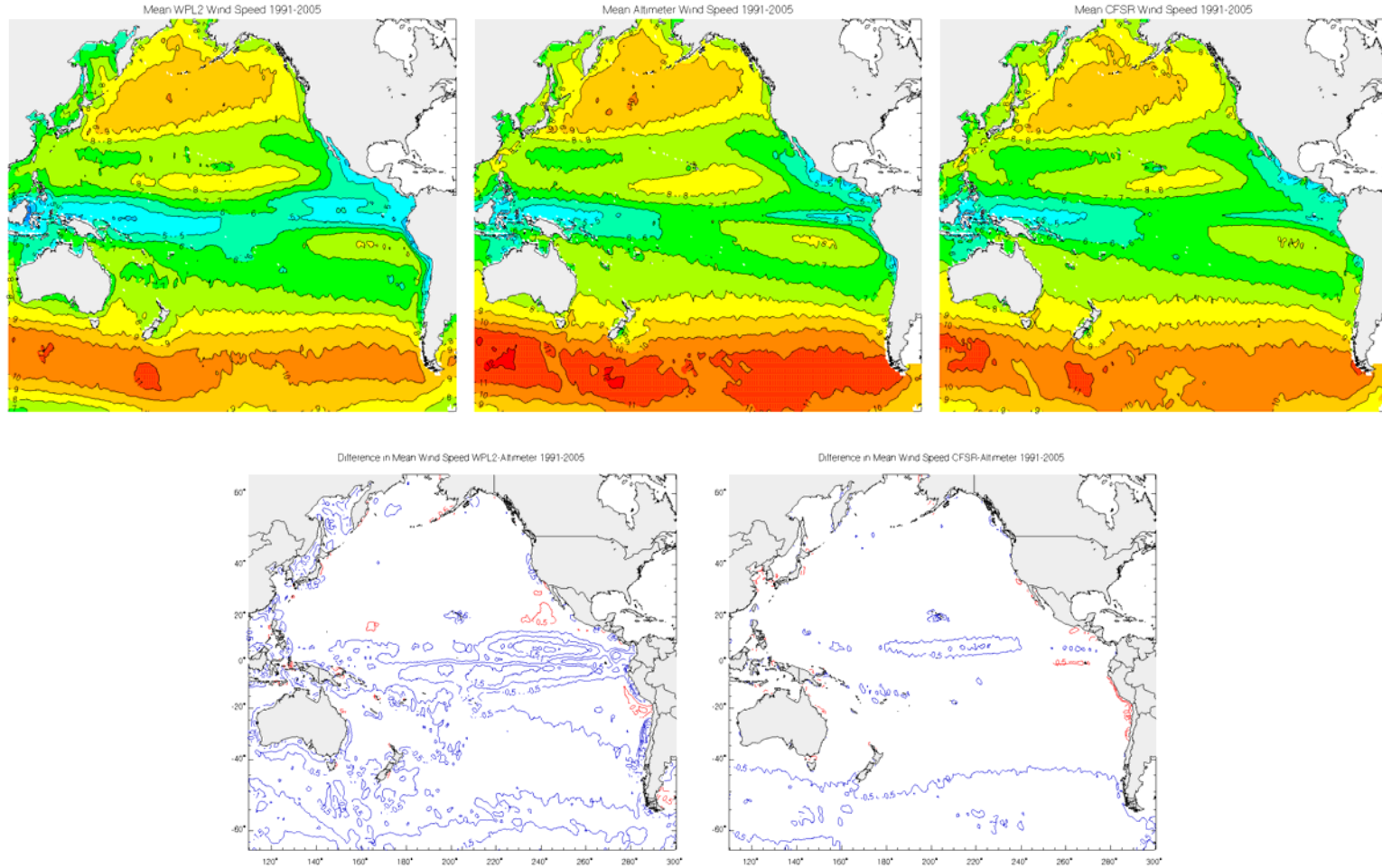|	Station	Number of Pts	Mean Meas	Mean Hind	Diff (H-M)	RMS Error	Stnd Dev	Scat Index	Corr Coeff
Wind Spd. (m/s)	WISPAC Level2	354421256	8.15	7.66	-0.49	2.40	2.35	0.29	0.82
Wind Spd. (m/s)	CFSR	336553877	8.20	7.98	-0.22	2.00	1.99	0.24	0.87

Figure 3 Mean wind speed (m/s) for WPL2 (top left), altimeter measurements (top, middle) and CFSR (top, right). Difference plots for WPL2-Altimeter (left) and CFSR-Altimeter (right) are shown below.

Table 3 WPL2/CFSR altimeter wind and wave statistics by buoy region for 2000/2004

	Station	Number of Pts	Mean Meas	Mean Hind	Diff (H-M)	RMS Error	Stnd Dev	Scat Index	Corr Coeff
Wind Spd. (m/s)	WPL2 2000	24498120	8.22	7.68	-0.53	2.23	2.17	0.26	0.82
Sig Wave Ht (m)	WPL2 2000	24496829	2.73	2.55	-0.18	0.74	0.72	0.26	0.86
Wind Spd. (m/s)	CFSR 2000	24498120	8.22	7.93	-0.29	1.73	1.70	0.21	0.89
Sig Wave Ht (m)	CFSR 2000	24496829	2.73	2.71	-0.02	0.58	0.58	0.21	0.92
Wind Spd. (m/s)	WPL2 2004	32169091	8.41	7.89	-0.52	2.11	2.04	0.24	0.85
Sig Wave Ht (m)	WPL2 2004	32167390	2.73	2.64	-0.09	0.67	0.67	0.24	0.88
Wind Spd. (m/s)	CFSR 2004	32169091	8.41	8.03	-0.38	1.63	1.59	0.19	0.91
Sig Wave Ht (m)	CFSR 2004	32167390	2.73	2.74	0.01	0.55	0.55	0.20	0.92

c. Winds in Tropical Systems

The CFSR modeling system includes a tropical system vortex track repositioning scheme as well as assimilation of historical storm reports (Saha *et al.* 2010). Despite these advances in inclusion of tropical systems, our study of many cases of tropical cyclone representation in the CFSR output suggests that direct use of CFSR in tropical events is not recommended for refined applications. CFSR is unable to represent the proper intensity or radius of maximum winds associated with each system, which are the two major factors in both wave and surge response. Certainly, the ~38 km resolution of the CFSR plays an important role in the lack of skill of the moderate/intense storms which normally display wind radii less than 38 km. However, even storms with radius of maximum winds greater than the CFSR grid spacing display bias.
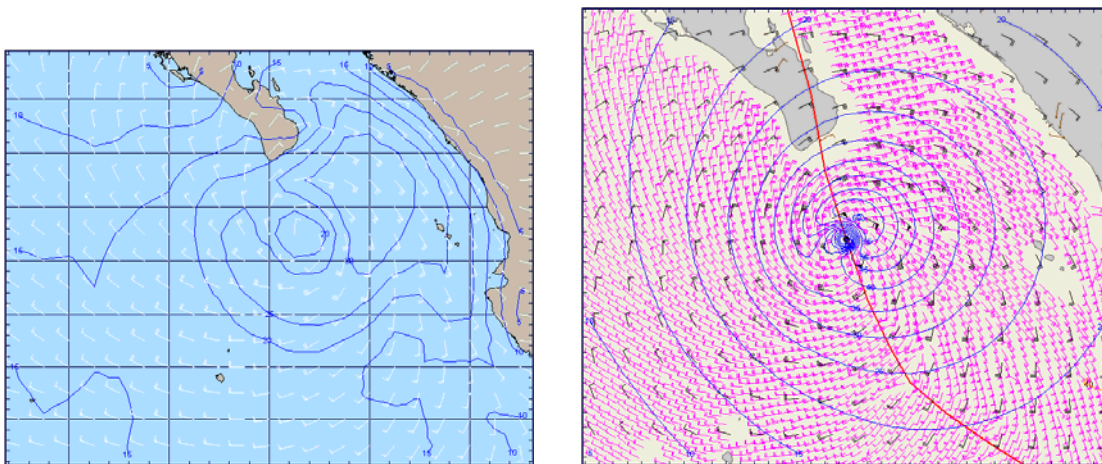

Figure 4 Wind fields from a tropical PBL model with QUIKSCAT barbs (left) and CFSR on WISPAC grid (right) valid during Henriette (Sept-04-2007 12 UTC)

To illustrate this deficiency we show a comparison of the CFSR representation (Figure 4, left) of a well developed tropical cyclone, in this case Hurricane Henriette (2007_11 in the NEPAC) valid Sept-04-2007 at 12 UTC. The CFSR wind field is compared to the representation of surface wind speed and direction provided by the application of a proven mesoscale cyclone model (Figure 4, right) forced by all in-situ, aircraft and satellite data typically available in the modern period. At the time shown, the system had an intensity of 60 knots (30-minute average), and associated radius of maximum winds of 40-45 km. The CFSR winds report a maximum wind of 36-40 knots with radius of maximum winds of 110-140 km. These relatively large differences typify the entire history of the storm.

A similar difference is displayed in Hurricane Isabel 2003 on Sept-17th (Figure 5). This figure shows the CFSR winds (left) compared to the HWnd analysis available from the Hurricane Research Division (HRD). The HRD HWnd analysis depicts a radius of maximum winds of 95 km with associated maximum wind of 84 knots (30-min. average) while CFSR depicts a radius of 125 km and maximum wind of just 68 knots.

The performance of the CFSR in tropical forcing is not an unexpected result as the reanalysis was never intended for such use. To produce credible wave hindcasts with tropical forcing it has been commonplace to overlay tropical forcing provided by either a proven mesoscale model or via the storm snapshots provided by HRD (appropriately modified for wind averaging period). Such a methodology has been extensively applied in global (GROW), regional (MSC 50) and storm specific hindcasts (see Swail *et al.* 2006 and Cardone *et al.* 2007) with great success. The inclusion of tropical systems within the CFSR does simplify the blending procedure as large differences in storm position are less likely than those found in R1/R2 products.
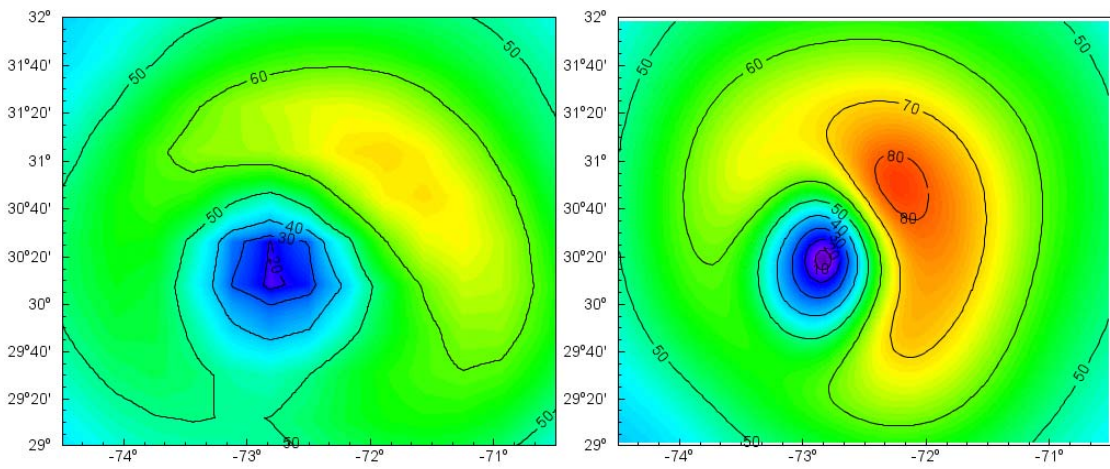

Figure 5 Comparison of wind speed (knots, 30-min average) for CFSR (left) and HWnd (right) valid 16:30 UTC 17-Sep-2003 during Hurricane Isabel

d. Performance in Extreme Extra-Tropical Storms

The database of Very Extreme Sea State (VESS) storms based on altimeter data (Cardone *et al.* 2011) provides a wealth of extra-tropical cases to extract and analyze the CFSR driven global hindcast. This dataset contains over 5000 individual altimeter segments for storm conditions greater than 12 meters. The storm segments displayed in Figure 6 depict some of the best comparisons between the altimeter and CFSR/OWI-3G hindcast. In each storm, the resulting hindcast represents both the slope and peak conditions of the altimeter measurements. Figure 7, on the other hand, illustrates some of the misses in the hindcast in which peak conditions are biased low by 5 meters or more in 10-15 meter events. Examples of both good and poor fits are found in all basins worldwide. Further work is underway as part of the VESS study to assess the meteorological characteristics of the VESS population which may prove useful in diagnosing storm types that are not handled well by the CFSR model.

The VESS database provides 184 cases of measured significant wave height above 16 m in the period covered by the CFSR/OWI-3G hindcast. Peak conditions measured in each of the 184 events were extracted and compared to the CFSR/OWI-3G hindcast. A scatter plot of the peak-to-peak conditions is shown in Figure 8. Overall, the CFSR/OWI-3G hindcast displayed a negative bias of 2.30 m for storms of this intensity.

In both the VESS and WISPAC study, a preliminary assessment of the wind fields in several of the storms was performed to attempt to determine the conditions in which the CFSR hindcast was unable to replicate the measured wave heights. Figure 9 illustrates a feature of the CFSR winds found in some of the strong extra-tropical storm systems. The figure shows the track of an extra-tropical system which exits the coast of Japan with central pressure of 980 mb. The low rapidly intensifies and just 36 hours later is a 944 mb system in the mid-Pacific. A comparison of the maximum winds associated with this system obtained from CFSR and a careful kinematic reanalysis of the storm display a tendency of the CFSR winds to lose energy in between passes of the QUIKSCAT scatterometer. Peaks in the CFSR winds are just after a QUIKSCAT pass and nearly match the kinematic analysis which applies the same data. In between scatterometer passes; the CFSR loses energy in the wind maxima. The resulting CFSR wave hindcast shows a negative bias in the peak wave conditions. This strong connection to the pass of a single instrument in some storm events is a concerning one, as it brings into question the homogeneity of the CFSR as wind observation platforms change over the years.
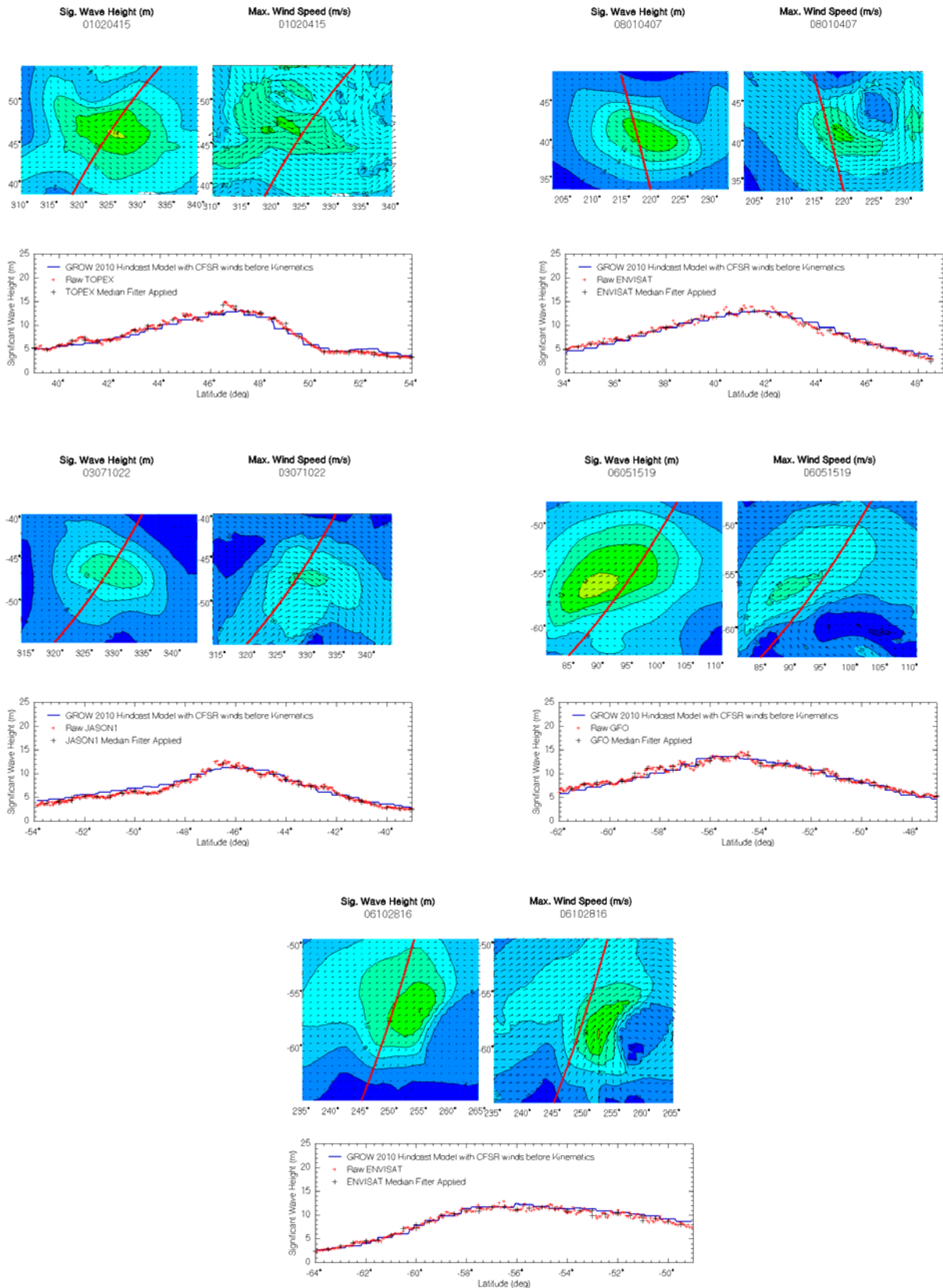
Figure 6 Examples of North Atlantic (left, top), North Pacific (right, top), South Atlantic (left,middle), South Indian (right, middle) and South Pacific (bottom) CFSR/OWI-3G wave height comparisons with altimeter measurements that display good agreement.
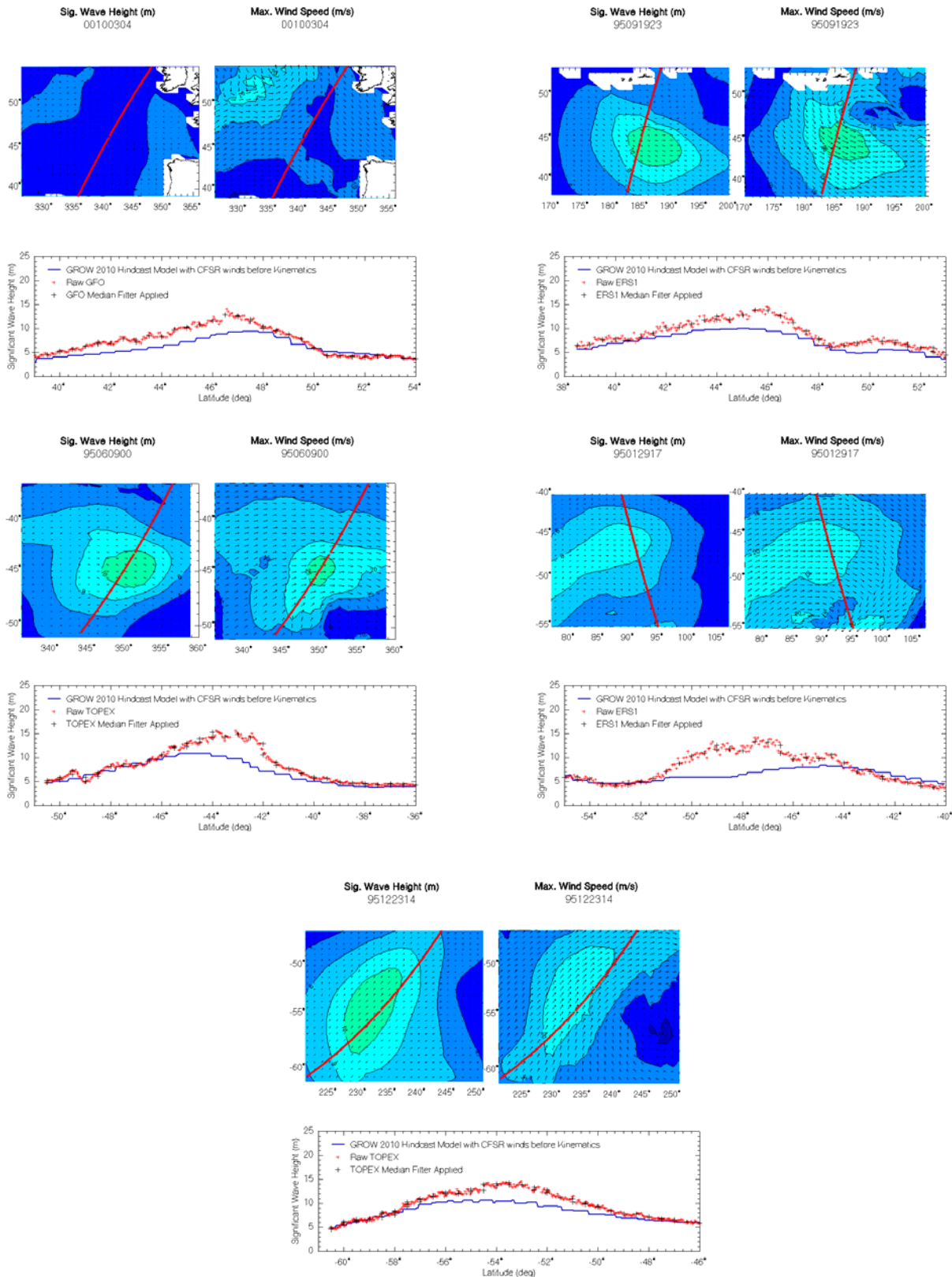
Figure 7 Examples of North Atlantic (left, top), North Pacific (right, top), South Atlantic (left,middle), South Indian (right, middle) and South Pacific (bottom) CFSR/OWI-3G wave height comparisons with altimeter measurements that display poor agreement.
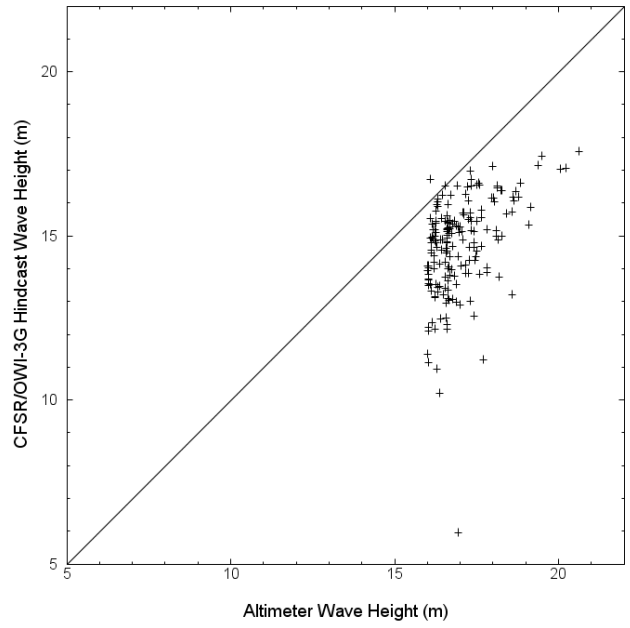
Figure 8 Comparison of hindcast and measured peak wave heights for altimeter storms greater than 16m
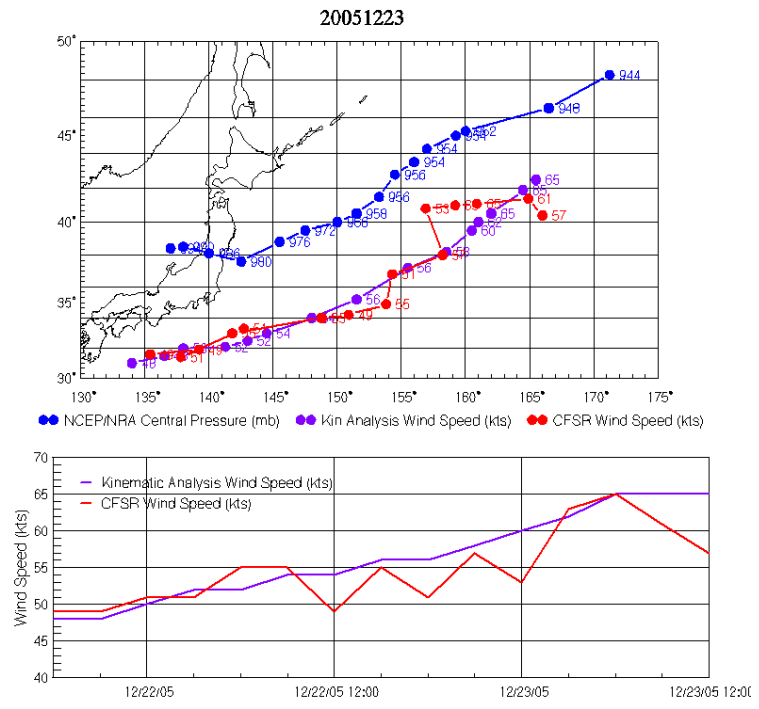

Figure 9 Comparison of CFSR and kinematic analysis maximum winds associated with a Dec-2005 North Pacific extra-tropical system.

Individual storms, even those that generate the highest significant wave heights in the VESS archive, can be reanalyzed using careful kinematic analysis. Figure 10 depicts the resulting

comparison of just such an analysis for a Feb-2007 extra-tropical storm in the North Atlantic from Cardone *et al.* 2011. Unmodified CFSR resulted in an underestimation of peak conditions by 3-4 meters, while the reanalyzed wind fields result in a wave field comparable with a median filter of the individual observations. Further work with the VESS database underway is attempting to identify VESS storms through their meteorological characteristics which could then be applied in the pre-altimeter period.
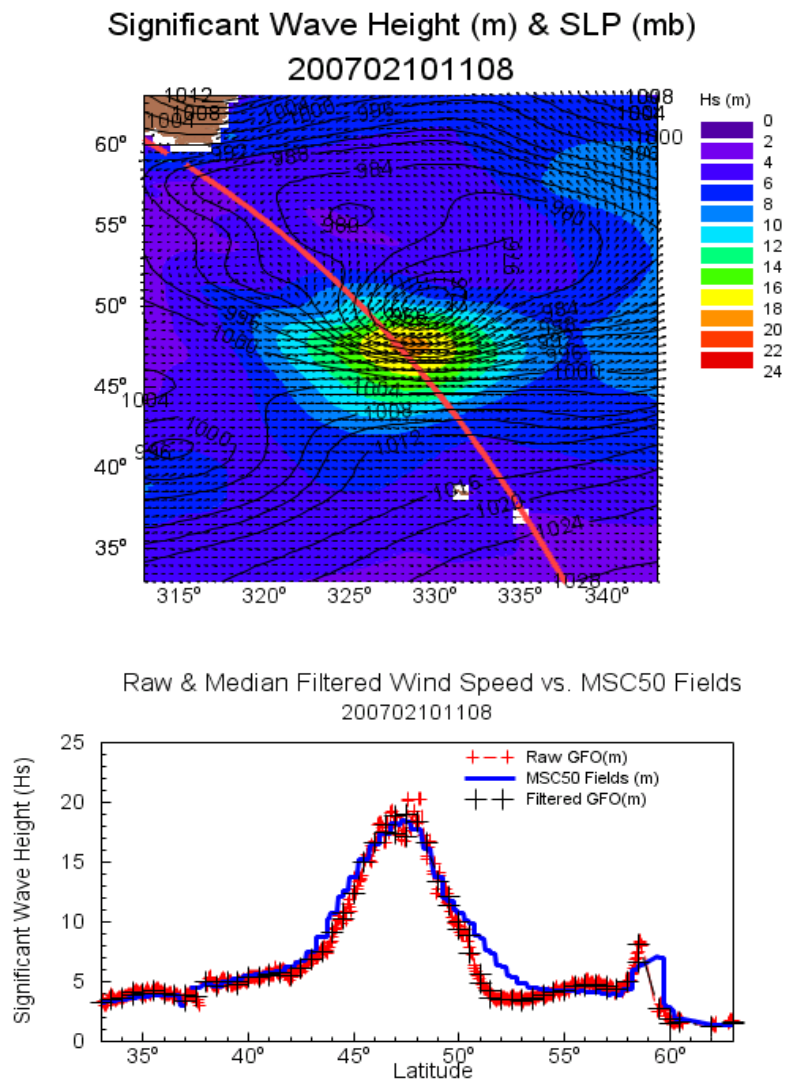

Figure 10 Comparison of performance of OWI-3G in VESS storm with kinematic reanalysis of CFSR wind fields. Color contoured significant wave height (m) with sea level pressures valid Feb-10-2007 at 11:08 UTC are shown above with the pass of the altimeter. Below depicts the hindcast and measured significant wave height along the pass. From Cardone *et al.* 2011.

e. Regional Use: Vietnam Case

During a hindcast project of a Southern South China Sea, a deficiency of swell energy was detected well offshore of Malaysia at a latitude of approximately 5 N during the cold season northeast monsoon regime. Detailed wind and wave measurements were made by a client on site (not shown) and the presence of the wave bias was confirmed by altimeter measurements. The hindcast had applied the original NCEP reanalysis as a base wind field with regional statistical corrections provided by time-matched model and QUIKSCAT scatterometer data. Tracing the wave energy backwards, it was determined the source zone was a coastal enhancement of the cold season northeast monsoon offshore Vietnam some 500 km north of the target site.

Figure 11 (upper) illustrates how poorly the unadjusted NRA winds perform when compared to the scatterometer pass valid at 23:00 UTC on Nov-14-2001. NRA winds in the core of the flow are 7-9 m/s while the measurements indicate a peak condition of 22 m/s. Comparison of CFSR winds at the same time (Figure 11, below) displays much more structure to the wind maxima, no doubt due to the increased resolution of the CFSR reanalysis. However, the peak conditions are still underestimated, with CFSR indicating only 12-13 m/s in the core. Interestingly, the CFSR wind field analysis valid at the next hour (Figure 12) show a better match with peak conditions in the 15-16 m/s range. This is most likely due to the inclusion of the 23:00 UTC scatterometer pass in the reanalysis.

When the wave hindcast was rerun using the CFSR forcing, the conditions at the target site did improve, but still under-predicted the wave conditions at the site. We believe there are two reasons for this: First, while they are an improvement over the unadjusted original reanalysis winds, the CFSR wind fields still under estimated the peak wind speeds in the core of the monsoonal flow. Secondly, an hour-by-hour comparison of CFSR winds shows a lack of continuity in the peak conditions such as that displayed in Figures 11 and 12. The reanalysis appears to make use of the scatterometer pass data, but is not able to maintain the peak wind structure in between passes for this case. This is an indication that continuity of the peak conditions found in the VESS storms is also apparent in certain forcing conditions which are not as extreme.

The hindcast solution to the monsoonal flow was to develop a series of training sets based on a number of select monsoon cases from the hindcast period. These events were kinematically reanalyzed using available insitu and satellite-based wind observations to develop specific corrections. Figure 13 shows the boxes of statistical corrections as well as a kinematic analysis of an event (Figure 13, right top) compared to a wind field derived from the hindcast (Figure 13, right bottom) with both basin-wide and monsoon season corrections. The resulting wave hindcast matched the client observations during the measurement period and removed the negative bias.
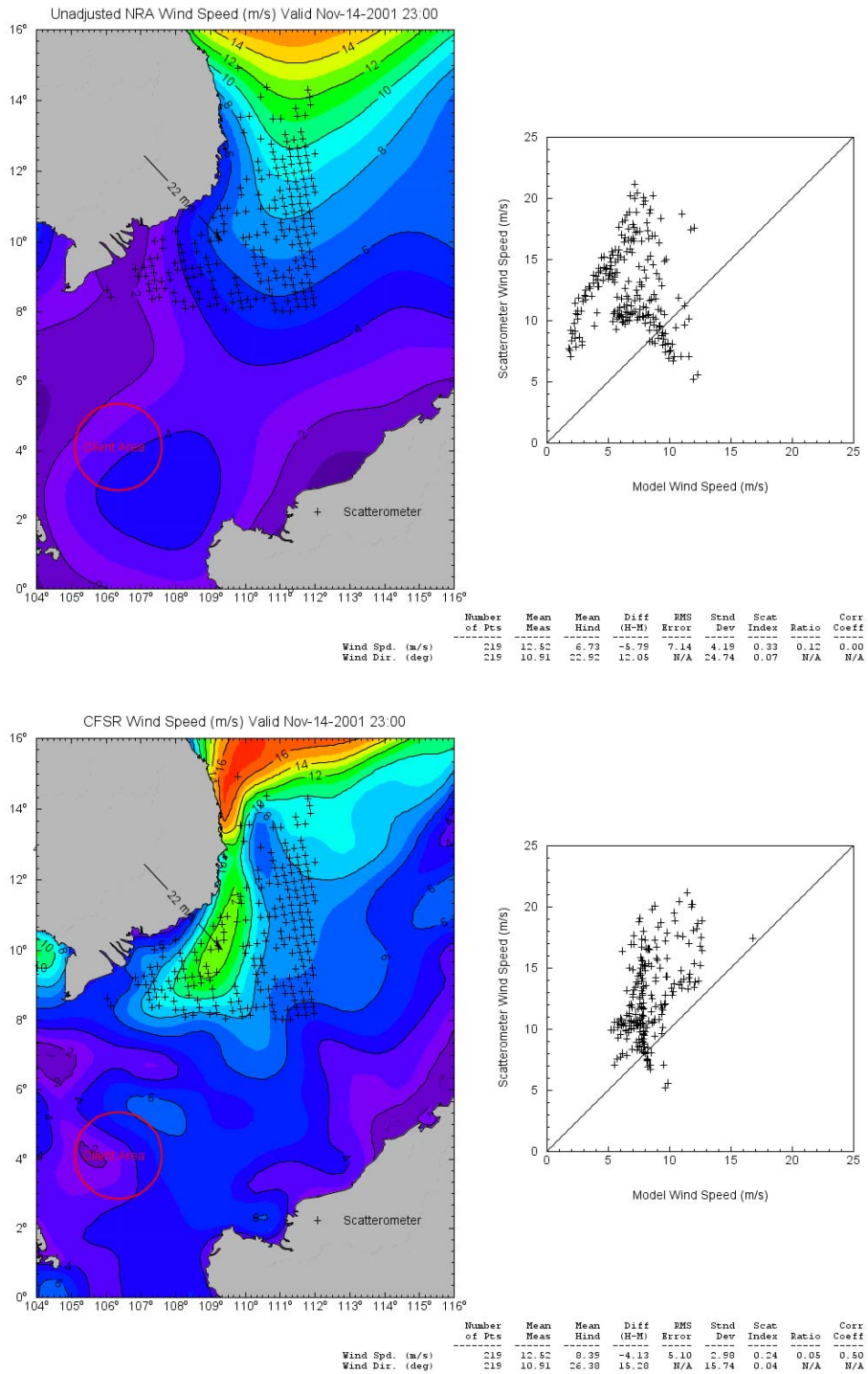
Figure 11 Comparison of modeled wind fields (unadjusted NRA above, CFSR below) when compared to scatterometer observations
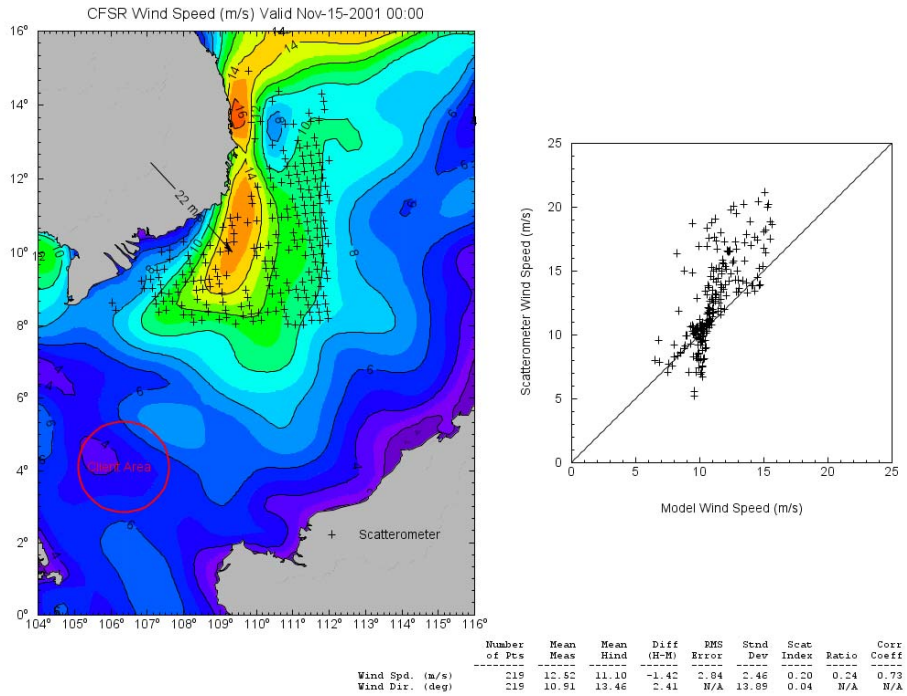
CFSR Wind Speed (m/s) Valid Nov-15-2001 00:00

	Number of Pts	Mean Meas	Mean Hind	Diff (H-M)	RMS Error	Stnd Dev	Scat Index	Ratio	Corr Coeff
Wind Spd. (m/s)	219	12.52	11.10	-1.42	2.84	2.46	0.20	0.24	0.73
Wind Dir. (deg)	219	10.91	13.46	2.41	N/A	13.89	0.04	N/A	N/A

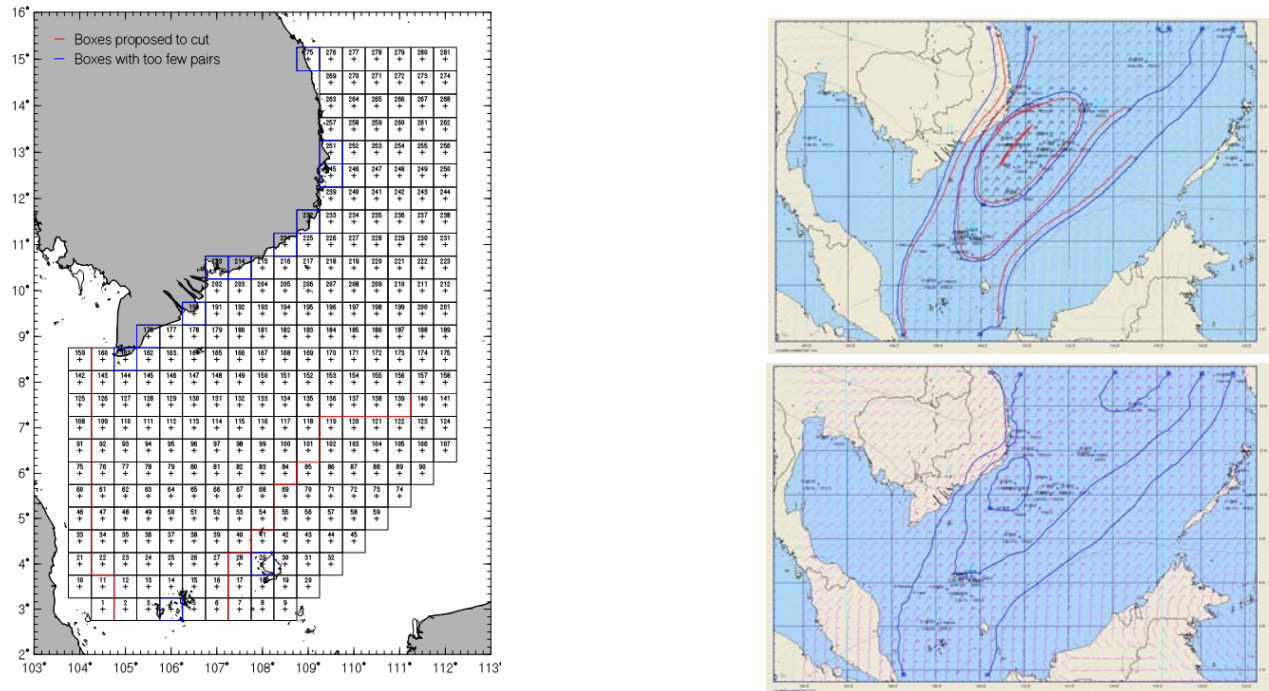**Figure 12 Comparison of CFSR valid at 15:00 compared to scatterometer pass at 14:23**

Figure 13 Regional statistical corrections applied in cold season monsoons (left) based on kinematically analyzed storms (top, right) with resulting wind field (bottom, left)

6. Conclusions and Recommendations

Overall, the CFSR 10 meter wind field provides an excellent source of forcing for a 3rd generation wave model. The skill of the base product appears to be on par with previous long-term continuous hindcast efforts such as the MSC50 which required significant reanalysis of R1/R2 products to obtain an increased level of skill. Users are cautioned about direct application of CFSR in tropical cyclones and extreme extra-tropical storms as the CFSR lacks both the resolution and ability to maintain the peak conditions exhibited in each. Standard hindcast practices such as inclusion of meso-scale driven forcing, statistical comparison/adjustment, and kinematic reanalysis of storm events continue to play an important role in producing wave climatologies for application in design and determination of extremes. Performance in specific areas may vary depending on the meteorological forcing even in non-extreme conditions, as shown by the Vietnam monsoon case. Application of CFSR for a particular site requires, as always, an assessment and critical knowledge of the applicability of the major wind forcing mechanisms pertinent to the local area.

There are a number of additional factors in the implementation of the CFSR hindcast which have implications for its use for long term wave climate production. The inclusion of scatterometer data post-1991 appears to have a large impact in some storm events. The impact on the marine forcing is twofold: first, the pass to pass behavior of the peak conditions makes it difficult to apply pure statistical corrections as have been proven successful in R1/R2 products. Second, it increases the risk of a step discontinuity between the period pre and post scatterometry. A second CFSR run from 1948-2010 without satellite assimilation is currently planned by NCEP and could address both issues. Lastly, unlike the R1/R2 efforts the frozen CFSR modeling system is not being extended past March 2011. Fields from April 2011 are being made available from Version 2 of the CFS system and only in real time (no archive is being planned). Further work will be required to assess any step changes in the marine winds from CFSR and CFS Version 2 output.

References

Cardone, V.J., J.G. Greenwood and M.A.Cane, 1990. *On trends in historical marinewind data.* J. Climate, 3, 113-127.

Cardone, V.J., H.C. Graber, R.E. Jensen, S. Hasselmann, and M.J. Caruso, 1995. *In search of the true surface wind field in SWADE IOP-1: ocean wave modeling perspective*. The Global Ocean Atmosphere System, **3**, 107-150.

Cardone, V.J., R.E. Jensen, D.T. Resio, V.R. Swail and A.T. Cox, 1996. *Evaluation of Contemporary Ocean Wave Models in Rare Extreme Events: "Halloween Storm of October, 1991; "Storm of the Century" of March, 1993."* J. Atmos. Ocean. Tech., **13**, 1, 198-230.

Cardone, V.J., A.T. Cox and G.Z. Forristall, 2007: *OTC 18652: Hindcast of Winds, Waves and Currents in Northern Gulf of Mexico in Hurricanes Katrina (2005) and Rita (2005).* 2007 Offshore Technology Conference, May 2007, Houston, TX.

Cardone, V.J., A.T. Cox, M.A. Morrone and V.R. Swail, 2011: Global Distribution and Associated Synoptic Climatology of Very Extreme Sea States (VESS). 12th International Workshop on Wave Hindcasting and Forecasting. October 31-November 4th, 2012, Kohala Coast, Hawaii.

Cox, A.T., and V.R. Swail, 2001. *A global wave hindcast over the period 1958-1997: validation and climate assessment.* J. of Geophys. Res.

Cox, A.T. and V.J. Cardone. *20 Years of Operational Forecasting at Oceanweather.* 7th International Workshop on Wave Hindcasting and Forecasting October 21-25, 2002, Banff, Alberta, Canada

Forristall, G.Z. and J. A. Greenwood, 1998. *Directional spreading of measured and hindcasted wave spectra.* Proc. 5th International Workshop on Wave Hindcasting and Forecasting, Melbourne, FL, January 26-30, 1998.

Greenwood, J.A., V.J. Cardone and L.M. Lawson, 1985. *Intercomparison test version of the SAIL wave model.* Ocean Wave Modelling, the SWAMP Group, Plenum Press, 221-233.

Kalnay, E., *et al*, 1996. *The NCEP/NCAR 40-Year reanalysis project*. Bull. AMS, 77(3), 437-471.

Khandekar, M.L., R. Lalbeharry and V.J. Cardone, 1994. *The Performance of the Canadian Spectral Ocean Wave Model (CSOWM) During the Grand Banks ERS-1 SAR Wave Spectra Validation Experiment.* Atmosphere-Ocean, **32**, 1, 31-60.

Saha, Suranjana, Shrinivas Moorthi, Hua-Lu Pan, Xingren Wu, Jiande Wang, Sudhir Nadiga, Patrick Tripp, Robert Kistler, John Woollen, David Behringer, Haixia Liu, Diane Stokes, Robert Grumbine, George Gayno, Jun Wang, Yu-Tai Hou, Hui-ya Chuang, Hann-Ming H. Juang, Joe Sela, Mark Iredell, Russ Treadon, Daryl Kleist, Paul Van Delst, Dennis Keyser, John Derber, Michael Ek, Jesse Meng, Helin Wei, Rongqian Yang, Stephen Lord, Huug van den Dool, Arun Kumar, Wanqiu Wang, Craig Long, Muthuvel Chelliah, Yan Xue, Boyin Huang, Jae-Kyung Schemm, Wesley Ebisuzaki, Roger Lin, Pingping Xie, Mingyue Chen, Shuntai Zhou, Wayne Higgins, Cheng-Zhi Zou, Quanhua Liu, Yong

Chen, Yong Han, Lidia Cucurull, Richard W. Reynolds, Glenn Rutledge, and Mitch Goldberg, 2010: *The NCEP Climate Forecast System Reanalysis*. Bull. of AMS, August 2010, 1015-1057.

Swail, V.R. and A.T. Cox, 2000. *On the use of NCEP/NCAR reanalysis surface marine wind fields for a long term North Atlantic wave hindcast*. J. Atmos. Ocean. Technol., **17**, 532-545.

Swail, V.R., V.J. Cardone, M. Ferguson, D.J. Gummer, E.L. Harris, E.A. Orelup and A.T. Cox, 2006 *The MSC50 Wind and Wave Reanalysis*. 9th International Wind and Wave Workshop, September 25-29, 2006, Victoria, B.C.

WAMDI Group, 1988. *The WAM model - a third generation ocean wave prediction model*. J. Phys. Ocean. **18**: 1775-1810.

Snyder, R., F.W. Dobson, J.A. Elliott and R.B. Long, 1981. *Array measurements of atmospheric pressure fluctuations above surface gravity waves*. J. Fluid Mech., **102**, 1-59.

Wu, J., 1982. *Wind-stress coefficients over the sea surface from breeze to hurricane*. J. Geophys. Res., **87**, 9704-9706.